Title

OXYGEN TRANSFER KINETICS BETWEEN Ga-Ga2O3 ELECTRODES AND THE SOLID ELECTROLYTE CALCIA-STABILIZED ZIRCONIA

Authors

Donaghey, L.F.
Pong, Raymond.

Publication Date

1973-08-01

Submitted to
Journal of the Electrochemical Society

LBL-1892
Preprint

OXYGEN TRANSFER KINETICS BETWEEN Ga-Ga_2O_3 ELECTRODES AND THE SOLID ELECTROLYTE CALCIA-STABILIZED ZIRCONIA

L. F. Donaghey and Raymond Pong

August 1973

Prepared for the U. S. Atomic Energy Commission
under Contract W-7405-ENG-48

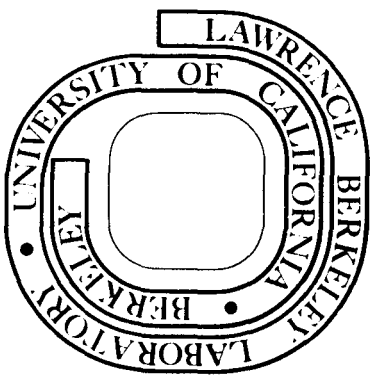

LBL-1892

DISCLAIMER

OXYGEN TRANSFER KINETICS BETWEEN Ga-Ga_2O_3 ELECTRODES AND THE SOLID ELECTROLYTE CALCIA-STABILIZED ZIRCONIA

L. F. Donaghey* and Raymond Pong†

Inorganic Materials Research Division of the
Lawrence Berkeley Laboratory and the
Department of Chemical Engineering of the
University of California, Berkeley
Berkeley, California 94720

Abstract

The kinetics of oxygen transfer between Ga-Ga_2O_3 composite electrodes and the solid electrolyte calcia-stabilized zirconia, ZrO_2(CaO), were studied with the symmetric, galvanic cell,

$$W \;/\; Ga\text{-}Ga_2O_3 \;/\; Ca_{0.15}Zr_{0.85}O_{1.85} \;/\; Ga\text{-}Ga_2O_3 \;/\; W,$$

over the temperature range from 800 to 900°C. Chronopotentiometric studies were conducted using current densities from 0.3 to 130 $\mu A/cm^2$ to obtain overpotentials for faradaic oxidation and reduction reactions at the Ga-Ga_2O_3 / ZrO_2(CaO) interface. A linear dependence of the overpotential on current density was obtained, corresponding to a local electrode resistance of 3.8 ohm per cm^2 of electrode-electrolyte interface at 800°C. The data is in agreement with a solution-diffusion mechanism of oxygen transport through liquid Ga in the electrode between the ZrO_2(CaO) electrolyte and Ga_2O_3 particles.

*Electrochemical Society, Active Member

†Electrochemical Society, Student Member

Key Words: emf measurements, solid electrolyte electrode properties, transfer kinetics

Introduction

Solid electrolytes have become important in recent years for use in thermodynamic and kinetic studies with solid state electrochemical cells (1-4) and more recently, in fuel cells and other power sources (5-11). Major areas of concern in kinetics and power source applications of solid electrolytes are the structure of the solid electrolyte-electrode interface and the electrochemical, rate-controlling process for ionic transport across this interface (12). Considerable theoretical and experimental work has been reported concerning space charge polarization in liquid and solid systems where it is well established that static concentration gradients of ionic species and diffuse, charged double-layers play an important roll (13-17). Most previous investigations of electrode processes in solid systems have been limited to single-phase electrodes (18) in asymmetric cells containing both non-polarizable and polarizable electrodes (19). In this paper studies of oxygen transfer between the two-phase, liquid metal-metal oxide electrode $Ga_{(\ell)}$- Ga_2O_3, and the solid electrolyte $ZrO_2(CaO)$ in a symmetric solid state galvanic cell are reported.

Oxygen transfer kinetics at interfaces between two-phase electrodes and solid electrolytes is important in many electrochemical applications. Metal-metal oxide mixtures are the most commonly used reference electrodes in thermodynamic studies with solid state galvanic cells (3), where electrode polarization is undesirable. Kinetic studies with such cells require oxygen transfer for coulombic titration experiments (20), for measurements of oxygen diffusion in liquid and solid metals (1, 3), and for phase boundary reaction rate determinations (21). Nevertheless, oxygen transfer kinetics from

oxygen transfer kinetics from metal-metal oxide electrodes to solid electrolytes has received relatively little study. Steele (22) studied the reversibility of several such electrodes. Recently, Worrell and Iskoe (23) measured steady-state overpotentials for oxygen transfer from $Cu\text{-}Cu_2O$, Fe-FeO and Ni-NiO electrodes to calcia stabilized zirconia (52), three of the most commonly employed reference electrode-electrolyte combinations used in solid-state electrochemical cell studies.

The $Ga\text{-}Ga_2O_3$ electrode has been important as a reference for gallium activity in thermodynamic studies employing $ZrO(CaO_2)$ solid state electrochemical cells (24, 25). Seybolt (24) used this metal-metal oxide electrode in a study of Ga activities in the Ni-Ga system. Klinedinst et al. (25) studied the Ga activities in the In-Ga system with this electrode. Applications of this electrode in thermodynamic studies of III-V compound alloys is currently under study by the present authors. The $Ga\text{-}Ga_2O_3$ electrode is representative of liquid metal-metal oxide electrodes which are of practical importance for providing stable reference activities in galvanic cells, and an understanding of oxygen transfer kinetics in this system should provide a basis for employing these electrodes in electrochemical systems.

Experimental

Materials

Gallium metal* of 99.9999% purity and Ga_2O_3 powder† (-325 mesh) of 99.99% purity for coexistence electrodes and the ZrO_2(CaO) electrolyte†† were obtained from commercial sources. High purity, recrystallized Al_2O_3 was used in the remaining components of the cell assembly. An inert purge gas manifold was constructed of stainless steel throughout with KEL-F sealed, bellows valves. Viton and rubber O-rings were employed in seals between steel and ceramic components.

Apparatus

The experimental cell configuration is shown schematically in Fig. 1. A closed-end, 0.64 cm diameter ZrO_2 (15 mol % CaO) solid electrolyte tube separated one electrode contained within it from a second Ga-Ga_2O_3 electrode supported on Ga_2O_3 powder within a 1.5 cm I.D. alumina crucible. This assembly was contained in a closed-end alumina reaction tube which was sealed at the top by an O-ring seal contained in a water-cooled stainless steel cap. The cap contained two additional O-ring seals through which the electrolyte tube, a thermocouple protection tube and a purge gas inlet tube passed. Both of these tubes were also sealed at their tops by O-ring closures to a purge gas manifold. The tube assembly was positioned in a Kanthal A-1 alloy resistance furnace whose temperature was regulated by a triac-controlled, integrating proportional controller. The cell temperature

---

*Cominco Co., Seattle, Wash.

†Alfa Inorganic.

††Zirconium Corp. of America, Solon, Ohio.

was held constant (±0.5°C) at the electrode assembly by a control thermocouple placed outside the alumina reaction tube. Convection in the liquid gallium was prevented by maintaining a vertical thermal gradient of 0.3°C/cm over the electrode assembly. Electrical interference from current transients in the furnace winding was prevented by encasing the reaction tube in an electrically grounded stainless steel tube to shield the electrode circuit from induced potentials.

The electrical circuit and purge gas manifold are shown schematically in Fig. 2. The emf of a chromel-alumel thermocouple used to measure the cell temperature was determined with a Leeds and Northrup K-3 potentiometric facility. The tungsten wire contacts to the Ga-Ga_2O_3 electrodes were passed through De Khotinsky cement and glass seals to isothermal copper connectors, then to coaxial cables. Cell currents were produced with an Electronics Measurements, Model C636 constant current power supply (G, Fig. 2). The ohmic component of the voltage response to current changes was measured with a dual beam Tektronic type RM35A oscilloscope with a high speed type G differential input preamplifier plug-in (A_2, Fig. 2). The cell emf was measured with a Keithley 610C electrometer (E, Fig. 2) having a sensitivity of ±0.02 mV and an offset current of 5×10^{-15}A.

Procedure

Following assembly, the cell was well purged with flowing argon. Both electrode compartments were leak tight, as checked with a He leak detector. The initially 99.998% pure Ar was purified by passing it through a Centorr gas-purification furnace containing Ti chips heated to 800°C. After thorough purging, the cell temperature was raised to the operating temperature at 75°C/hr to minimize thermal stress on the ZrO_2(CaO) electrolyte. The cell was

equibrated overnight at the working temperature to anneal the electrodes and to allow a check on cell emf stability. During measurements both electrode compartments were sealed off from the gas manifold to prevent emf errors from gas flow sources.

Experiments were conducted with constant current density pulses between 0.3 and 130μA/cm^2. The open cell voltage was measured after equilibration and before current was applied. The ohmic voltage was measured from the abrupt change in oscilloscope trace occurring when the current to the cell was applied or terminated. Following the onset of each pulse the cell voltage was monitored intermittently for a period of 10-20 minutes during which the current was applied, followed by intermittent voltage measurements with no current for an additional 10-30 minute period, during which equilibrium was established. After all experiments were completed the cell temperature was lowered at 70°C/hr under flowing Ar. The cell was then dismantled for inspection of the electrodes and electrode-electrolyte interface to insure that the electrode remained two-phase during the experiments, and that wetting of the electrolyte by liquid gallium had occurred.

Results

Chronopoteniometric studies were carried out with the cell,

$$W / Ga_{(\ell)} - Ga_2O_3 \; / \; Zr_{0.85}Ca_{0.15}O_{1.85} \; / \; Ga_{(\ell)} - Ga_2O_3 / W. \quad [I]$$

Wagner (1) has shown that the cell emf is a function of the oxygen partial pressure at the two electrode-electrolyte interfaces,

$$emf = \frac{RT}{4F} \int_{\ell n P''_{O_2}}^{\ell n P'_{O_2}} t_{ion} \, d \, \ell n \, P_{O_2}, \quad P'_{O_2} > P''_{O_2} \qquad (1)$$

where t_{ion} is the ionic transference number. Thus, for the symmetric cell [I] at equilibrium, the cell emf should be zero. In practice, however, a small emf, V_0 can arise from small differences in temperature, composition or ambience between the two electrodes. When a current density i is passed through the cell, an oxygen ion flux of magnitude i/2 flows in the opposite direction for which an ohmic voltage component $L\rho i$ appears across the electrolyte of thickness L and resistivity ρ. In addition a local overpotential η appears at each of the two electrode-electrolyte interfaces which, for small oxygen partial pressure gradients, are

$$\eta' = \frac{RT}{4F} \ln\left(P'_{O_2}/P'^{e}_{O_2}\right) \tag{2a}$$

$$\eta'' = \frac{RT}{4F} \ln\left(P''_{O_2}/P''^{e}_{O_2}\right)^{-1} \tag{2b}$$

where $P'^{e}_{O_2}$ and $P''^{e}_{O_2}$ are the oxygen partial pressures far from the electrolyte in electrodes 1 and 2, respectively. Thus, the cell voltage measured during current flow is

$$V = V_0 + \eta' + \eta'' + L\rho i \tag{3}$$

The total, steady-state overpotential $\eta_t = \eta' + \eta''$ is a function of current density whose magnitude depends on the oxygen transfer kinetic mechanism. The magnitude of $\eta_t(i)$, and thus information on this mechanism, is readily deduced from V(i) measurements and independent determinations of V_0, L and ρ.

The cell voltage response to a long galvanostatic pulse is shown schematically in Fig. 3a. The experimentally measured voltages during, and following a pulse of $56\mu A/cm^2$ are shown in Figs. 3b and 3c, respectively. The data is plotted as a function of the square root of the incremental time following the current change to show the parabolic time dependence of the voltage transients.

The total steady-state overpotential η_t was calculated for each chronopotentiometric experiment from the magnitude of the galvanostatic voltage transient ($V_3 - V_2$, in Fig. 3a). The dependence of η_t on current density passed through the cell at 800°C is shown in Fig. 4. Measurements at current densities well above 100μA/cm^2 were hindered by the failure of the overpotential to reach steady state in a convenient period of time. On the other hand, measured overpotentials below ∿25μV were in error because of the finite noise level in the measurement circuit. A linear dependence of η_t on i was observed which, at 800°C, had a slope of 7.6 ± 2 ohm per cm^2 of electrode-electrolyte interface. Measurements of steady-state overpotentials at 900°C also showed a linear dependence of η_t on i with a slope of 4 ± 2 ohms per cm^2 of interface.

Discussion

Oxygen Transfer Mechanisms

During passage of current between electrodes, charge-carrying oxygen ions are transferred across the solid electrolyte. Gallium oxidation occurs at the positive cell electrode and oxide reduction, at the negative electrode.

Several mechanisms for oxygen transfer between the electrodes operate in parallel, and these are summarized in Fig. 5. Oxygen flowing from the solid electrolyte into liquid gallium supersaturates the metal after charge transfer. In the solution-diffusion mechanism (I) the dissolved oxygen diffuses across a narrow liquid layer to an oxide surface where oxidation is assumed to take place. The oxide can form on the solid electrolyte if a nucleation and growth mechanism (II) is operative. Alternately, the dissolved oxygen can adsorb onto and diffuse along the solid electrolyte-liquid metal interface (III) to an oxide grain contacting the

electrolyte. At points of three phase contact a metal-oxide-electrolyte reaction mechanism (IV) can operate without diffusion.

Oxygen transfer across the electrolyte-oxide interface can also occur by point defect migration through the oxide. For the anion diffusion mechanism (V) interstitial oxygen ions diffuse to metallic regions, or alternately, oxygen vacancies diffuse from the metal following local oxidation toward the electrolyte. In the cation diffusion mechanism (VI), interstitial cations diffuse from the metal to the electrolyte where oxidation displaces the oxide phase in the direction away from the solid electrolyte.

Each oxygen transfer mechanism involves the series of kinetic steps. The charge transfer and oxidation processes are common to all oxygen transfer mechanism, while dissolution and liquid-phase or solid-state diffusion are required by several. Usually one step will be rate limiting.

Several of the oxygen transfer mechanisms do not contribute significantly to the total oxygen flux. Oxide nucleation by mechanism (II) cannot operate at sufficiently low oxygen supersaturation of the liquid phase (10^{-2} in this study). The oxygen solution-interface diffusion mechanism (III) is probably rate limited by the interfacial diffusion process for which the interfacial oxygen permeability is less than that for the bulk liquid phase. The extent to which the metal-oxide-electrolyte reaction mechanism (IV) can operate is limited by the amount of oxide contacting the electrolyte.

For the oxygen transfer mechanisms (V and VI), diffusive transport of point defects should be rate limiting. Cation interstitial diffusion is known to predominate over anion diffusion mechanisms in Ga_2O_3. In a study of the oxidation kinetics of GaAs (27), an oxide film of Ga_2O_3 was found to form after evaporation of arsenic. Further oxidation proceeds by interstitial diffusion of Ga through the oxide layer. This mechanism is

corroborated by Rosenberg (28) for InSb oxidation. The Sb remains metallic because the diffusivity of Sb as well as oxygen is much lower than that of the trivalent metal in the oxide. Thus, the anion diffusion mechanism (V) is virtually inoperative compared to the cation diffusion mechanism (VI). The cation diffusivity of the oxide, however, is significantly lower than the oxygen diffusivity of liquid gallium (29).

A study of the mechanisms shown schematically in Fig. 5 indicates that the solution-diffusion mechanism (I) should predominate in the temperature range studied, owing to the large permeability of liquid gallium. This mechanism is explored in the following section.

The Solution-Diffusion Model

The solution-diffusion model for aqueous reactions between sparingly soluble reagents and conducting electrodes has been investigated extensively by Dunning et al. (30), and studied experimentally by Katan et al. (17). The numerous local complex reaction paths operating at the electrode-electrolyte interface can easily be combined by expressing the overall rate constant k as a function of the rate constants for the i^{th} step, k_i,

$$k = \left[\sum_i A_i k_i^{-1}\right]^{-1} \qquad (4)$$

The numerical value of the coefficients, however, must be determined experimentally, unless the rate controlling step can be deduced by relative magnitude estimates. Such estimates suggest that liquid-phase diffusion of dissolved oxygen is rate controlling in the Ga-Ga_2O_3 electrode, and thus the overall rate constant k is approximately D_O, the diffusivity of oxygen in liquid gallium. This estimate of the rate controlling step is supported by a recent study of oxygen transfer between solid metal-metal oxide electrodes and solid electrolytes, where oxygen diffusion in the metal was found to be rate controlling (23).

Oxygen transport through the experimental cell by mechanism (1) under a galvanostatic driving force is shown schematically in Fig. 6. The overpotential at each electrode can be calculated from Eqs. 2 and 3 with the oxygen partial pressures at the electrolyte surfaces, P'_{O_2} and P''_{O_2}, and from the equilibrium partial pressures at the metal-metal oxide interfaces within the electrode, $P'^{e}_{O_2}$ and $P''^{e}_{O_2}$. The average partial pressure drops within the electrodes can be defined by $\overline{\Delta P}' = P'_{O_2} - P'^{e}_{O_2}$ and $\overline{\Delta P}'' = P''^{e}_{O_2} - P''_{O_2}$. The electrode overpotentials in the electrodes are then

$$\eta' = \frac{RT}{4F} \ln\left(1 + \frac{\overline{\Delta P}'}{P'_{O_2}}\right) \simeq \frac{RT}{4F} \frac{\overline{\Delta P}'}{P'_{O_2}} \tag{5a}$$

$$\eta'' = \frac{RT}{4F} \ln\left(1 - \frac{\overline{\Delta P}''}{P''_{O_2}}\right)^{-1} \simeq \frac{RT}{4F} \frac{\overline{\Delta P}''}{P''_{O_2}} \tag{5b}$$

The oxygen partial pressures can be converted to oxygen molar solubilities by Sievert's Law from which it follows, for the reaction $O_2 \longrightarrow 2O_{diss.}$, that the solubility is proportional to P_{O_2}, and therefore, $\Delta c/c = \frac{1}{2} \Delta P/P_{O_2}$.

The oxygen solubilities at the electrolyte surfaces will differ from the equilibrium solubility c_0 at the cell temperature. However, in the limit of small supersaturations, the overpotential for electrode 1 becomes

$$\eta' = \frac{RT}{2F} \frac{\overline{\Delta c}'}{c_0} \tag{6}$$

The oxygen ion molar flux J is related to the cell current density by Faraday's law, which for divalent ions is $it_{ion} = 2FJ$. The oxygen flux within the electrode metal phase is related to the oxygen diffusivity by Fick's first law,

$$J = -D \left.\overline{\frac{\partial c}{\partial z}}\right|_{z=0} = D \frac{\overline{\Delta c}}{\ell} \qquad (7)$$

where $\overline{\partial c/\partial z}$ is the average concentration gradient at the electrolyte and ℓ is a characteristic length. The dependence of the solubility drop on cell current is then

$$\overline{\Delta c} = \frac{i\, t_{ion}\, \ell}{2FD} \qquad (8)$$

Finally, the dependence of the electrode overpotentials on cell current is obtained by combining Eqs. 6 and 8,

$$\eta' = \frac{RT\, \ell'}{4F^2 Dc_O}\, t_{ion}\, i \qquad (9)$$

An identical expression applies to the second electrode. The ratio η'/i is the specific electrode resistance R_η'.

All coefficients in Eq. 9 are experimentally known except for the oxygen permeability of liquid gallium, Dc_O, and the characteristic diffusion lengths, ℓ'.

The oxygen permeability of liquid gallium can be deduced from the measured oxygen solubility c_O and the liquid-phase diffusivity D. The solubility of Ga_2O_3 in liquid gallium was determined by Foster and Scardefield (30) by a gravimetric method over the temperature range from 900 to 1200°C. Their experimental data on oxide mole fraction is represented here by the relation

$$x_{Ga_2O_3} = 1.175 \times 10^2 \exp\left[(-35{,}850 \pm 1{,}140)/RT\right] \qquad (10)$$

The solubility of atomic oxygen is then found by assuming that the dissolved oxide dissociates into atomic components, from which it follows that the molar solubility $c_O (\cong 3\, x_{Ga_2O_3} d_{Ga}/M_{Ga})$ is

$$c_0 = 30.63 \exp [(-35,850 \pm 1,140)/RT] \quad (11a)$$

The activation energy for dissolution is 35,850±1,140 cal for the available data, and thus the extrapolation of the oxygen solubility to low temperatures produces an error which increases with the extent of extrapolation. The diffusivity of oxygen in liquid gallium was measured by Klinedinst (29) by galvanostatic titration experiments. The diffusion coefficient was expressed by the equation,

$$D_{O,Ga_{(\ell)}} = (3.68 \pm 0.42) \times 10^{-3} \exp[(-8,370 \pm 0.25)/RT] \quad (11b)$$

The permeability of atomic oxygen in liquid gallium is, finally,

$$Dc_0 = 0.11273 \exp [(-44,220 \pm 1,140)/RT] \quad (12)$$

Thus, the permeabilities at 800 and 900°C are 1.11×10^{-10} and 6.49×10^{-10}, respectively.

A general dependence of the local overpotential on temperature and current density for the solution diffusion model can now be found by combining the permeability Eq. 12 with Eq. 9, for $t_{ion} \simeq 1$,

$$\eta' = (1.98 \times 10^{-9})\ \ell' i\ T \exp(44220/RT) \quad (13)$$

Again, the diffusion length ℓ' depends on the electrode structure. The $Ga\text{-}Ga_2O_3$ electrode resistivity associated with the local overpotential can be defined by

$$\rho_{\eta'} \equiv \frac{\eta'}{\ell' i} = (1.98\ 10^{-9})T \exp(44220/RT). \quad (14)$$

Unlike the overpotential resistance per unit area ($R_{\eta'} = \eta/i$), the local electrode resistivity is independent of the electrode structure, and is a property of the oxygen transfer through the liquid phase.

$Ga\text{-}Ga_2O_3$ Electrode Properties

If the solution-diffusion mechanism controls oxygen transfer between $Ga\text{-}Ga_2O_3$ electrode and the solid electrolyte with dissolved oxygen diffusion in liquid gallium as the rate controlling step, then the interfacial transfer resistivity ρ_η' should be given by Eq. 14. This rate control can be tested by comparing experimental data for η'/i with ρ_η', calculated from Eq. 14. The effective diffusion length required is then given by

$$\ell' = \rho_\eta^{-1} (\eta'/i)_{exp}. \tag{15}$$

At 800°C ρ_η equals 2162 ohm-cm, whereas the measured η'/i is 3.8 ohm-cm^2. The diffusion length deduced from these data is then

$$\ell' = 1.76 \times 10^{-3} cm.$$

This diffusion length is consistent with the actual electrode structure in which loosely packed Ga_2O_3 particles with an average diameter of 2.5×10^{-3}cm are infused with liquid gallium. The experimental data at 900°C indicates an effective diffusion length of 5.0×10^{-3} which is somewhat larger than expected for diffusion limited kinetics, but within the limits of error and reproducibility of the electrode structure.

Another test of the mechanism and rate control lies in the time dependence of the overpotential following initiation of a constant cell current. Transport of oxygen ions through the electrolyte causes a local supersaturation of dissolved oxygen which, in the quasi-steady state, can be shown to be related to the diffusion flux J and time t by

$$\Delta c \simeq J\sqrt{2t/D.} \tag{16}$$

The time dependence of the local electrode overpotential is then

$$\eta'(t) \propto \eta'(\infty)\sqrt{2Dt} \; / \; \ell' \; . \qquad (17)$$

A linear dependence of η' on $t^{1/2}$ for short times was observed in all experiments, again supporting the diffusion limited kinetics.

The measured overpotentials were independent of the direction of current flow to within 5%. The asymmetry of the experimental cell was minimized by limiting the interfacial area of the outer electrode in contact with the electrolyte tube. The dependence of overpotential on the direction of current flow is assumed to indicate differences in oxide packing within the two $Ga\text{-}Ga_2O_3$ electrodes.

The total oxygen flux transferred during the experiments is not expected to significantly alter the electrode structure at the solid electrolyte interface according to mechanism I. A calculation, based on the fact that 1 coulomb passing through the cell transfers 5.18×10^{-6} moles of oxygen, shows that an oxide thickness of only 200 Å per cm^2 of electrode-electrolyte interface was transferred during all experiments. For the idealized interface structure shown in Fig. 6, the ratio of oxide-metal area to metal-electrolyte area is 2.5, and thus the average oxide-metal interface displacement is only 80 Å. Most of the oxide-metal interface displacement takes place near the electrolyte where the diffusion distance is short, however, and this effect leads to the current-modified electrode structure shown in Fig. 6b. For the actual electrode containing irregular oxide particles in a liquid matrix, the oxide transfer processes has less effect on the electrode structure because of limited three-phase contact.

A comparison of the present results with earlier studies shows that the $Ga\text{-}Ga_2O_3$ electrode exhibits an exceptionally low overpotential-associated resistance. Worrell and Iskoe (23) have measured the dependence of steady-state

overpotentials on cell current for symmetric cells of the type, $M\text{-}MO_n$ / $ZrO_2(CaO)$ / $M\text{-}MO_n$, in which the $M\text{-}MO_n$ electrodes were Ni-NiO, Fe-FeO and $Cu\text{-}Cu_2O$. The steady-state overpotentials per unit area of electrode-electrolyte interface calculated from their data are shown in Fig. 7 along with the measurements from this study. From this comparison it can be seen that the $Ga\text{-}Ga_2O_3$ electrode exhibits a lower electrode overpotential than do the three most commonly employed reference electrodes and, therefore, promises to be a superior reference electrode for kinetics and phase equilibria applications in the low partial pressure range.

Acknowledgments

The financial support of the U. S. Atomic Energy Commission is gratefully acknowledged. The authors wish to thank Dr. W. L. Worrell for copies of his manuscripts prior to publication.

References

1. D. O. Raleigh in "Progress in Solid State Chemistry," Vol. III, H. Reiss, Ed., Pergamon Press, New York, N. Y., 1967, Chapter 3.
2. C. B. Alcock, Ed., "Electromotive Force Measurements in High-Temperature Systems," American Elsevier Publishing Co., New York, N.Y., 1968.
3. R. A. Rapp and D. A. Shores in "Physicochemical Measurements in Metals Research, Part 2," R. A. Rapp, Ed., Wiley-Interscience, New York, N. Y., 1970, p. 123.
4. H. Schmalzreid and A. D. Pelton, "Ann. Review of Mat. Sci.," Vol. 2, R. Huggins, Ed., Ann. Review Inc., Palo Alto, California, 1972, p. 143.
5. B. Reuter and K. Hardel, Naturwiss., 48, 161 (1961).
6. T. Takahashi and O. Yamamoto, Electrochim. Acta, 11, 779 (1966).
7. J. N. Bradley and P. D. Greene, Trans. Farad. Soc., 62, 2069 (1966); 63, 424 (1967).
8. B. B. Owens and G. R. Argue, Science, 157, 308 (1967).
9. R. T. Foley, J. Electrochem. Soc., 116, 13C (1969).
10. H. Wiedersich and S. Geller, "Chemistry of Extended Defects in Non-Metallic Solids," Proc. Symp. Scottsdale, Ariz., April 21, 1969.
11. W. van Gool, Ed., "Fast Ion Transport in Solids; Solid State Batteries and Devices," North-Holland Publishing Co., Amsterdam, 1973.
12. N. H. Michael and A. A. Pilla, J. Electrochem. Soc., 118, 72 (1971).
13. F. C. Anson, J. Phys. Chem., 71, 3605 (1967).
14. C. G. J. Baker and E. R. Buckle, Trans Faraday Soc., 64, 469 (1968).
15. R. P. Buck, J. Electroanal. Chem., 23, 219 (1969).

16. J. R. Macdonald, Trans. Faraday Soc., 66, 943 (1970).

17. T. Katan, S. Szpak and D. N. Bennion, J. Electrochem. Soc., 120, 883 (1973).

18. D. O. Raleigh in "Electroanal. Chem. - A Series of Advances," Vol. VI, A. J. Bard, Ed., Marcel-Dekker Press, New York, N. Y., 1967, pp. 87-186

19. S. V. Karpachev and A. T. Filyaev, Elektrokhimiya, 2, 617 (1966); 4, 498 (1968).

20. B. C. H. Steele in "Mass Transfer in Oxides," J. B. Wachtman and A. D. Franklin, Eds., N. B. S. Spec. Publ. 296, 1968 , p. 165.

21. F. A. Kröger, J. Electrochem. Soc., 120, 75 (1973).

22. B. C. H. Steele, in C. B. Alcock, Ed.,"Electromotive Force Measurements in High-Temperature Systems," Inst. of Mining and Met. Pub., London, 1968 , pp. 17-18.

23. W. L. Worrell and J. L. Iskoe, in W. van Gool, Ed., "Fast Ion Transport in Solids, Solid State Batteries and Devices," North-Holland Publ. Co., Amsterdam, 1973 , p. 513.

24. A. U. Seybolt, J. Electrochem. Soc., 111, 697 (1964).

25. K. A. Klinedinst, M. V. Rao and D. A. Stevenson, J. Electrochem. Soc., 119, 1261 (1972).

26. C. Wagner, Z. Physik. Chem., B21, 25 (1933).

27. H. T. Minden, J. Electrochem. Soc., 109, 733 (1962).

28. A. J. Rosenberg, J. Phys. Chem. Solids, 14, 175 (1960).

29. K. A. Klinedinst and D. A. Stevenson, J. Electrochem. Soc., 120, 304 (1973).

30. L. M. Foster and J. Scardefield, J. Electrochem. Soc., 116, 494 (1969).

List of Symbols

c_0 molar solubility, moles/cm^3

D diffusion coefficient, cm^2/sec

F Faraday constant, 96,489 coulomb/equiv., or 23,061 cal/volt-equiv.

J oxygen ion flux, moles/cm^2-sec.

L electrolyte thickness, cm

ℓ' characteristic diffusion length, cm

P_{O_2} oxygen partial pressure, atm

R gas constant, 1.987 cal/mole °K

R_{η}' local electrode resistance, ohm

T absolute temperature, °K

t_{ion} ionic transference number

V cell voltage, V

V_0 open cell voltage, V

x_i mole fraction of component i

η' local electrode overpotential, V

η_t total cell overpotential, V

ρ electrolyte resistivity, ohm-cm

ρ_{η} local electrode resistivity, ohm-cm

τ relaxation time constant, sec

List of Figures

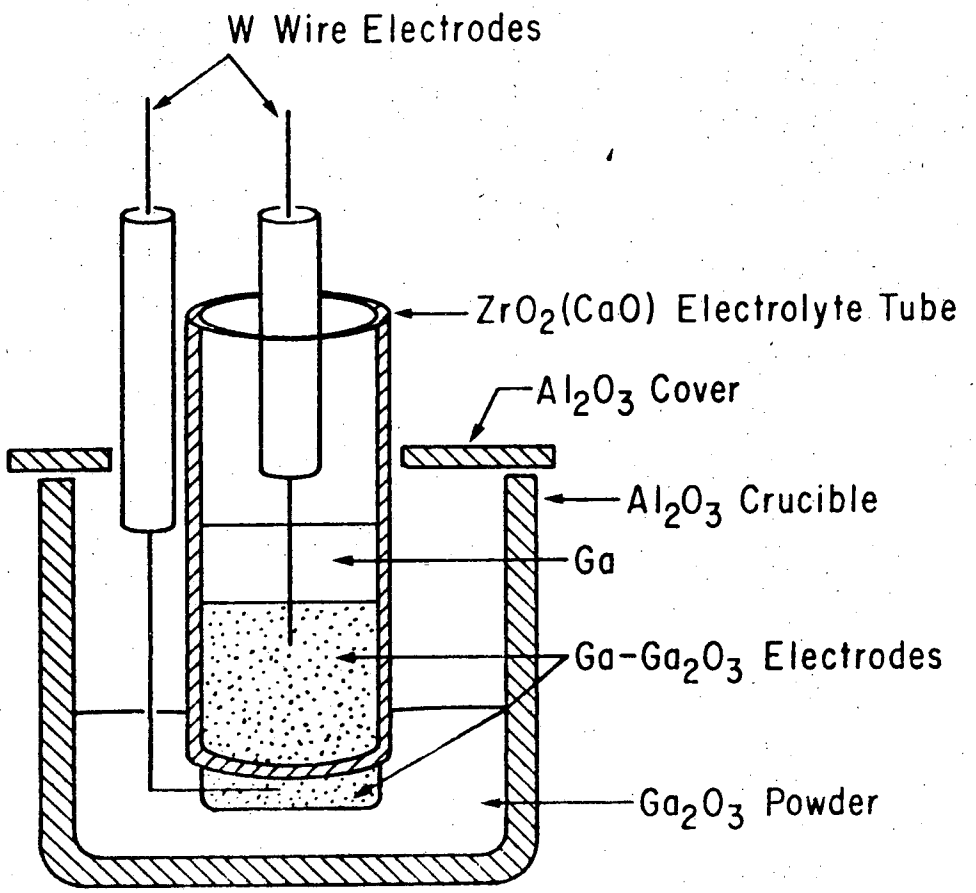
W Wire Electrodes
$ZrO_2(CaO)$ Electrolyte Tube
Al_2O_3 Cover
Al_2O_3 Crucible
Ga
Ga-Ga_2O_3 Electrodes
Ga_2O_3 Powder
XBL737-1568

Fig. 1

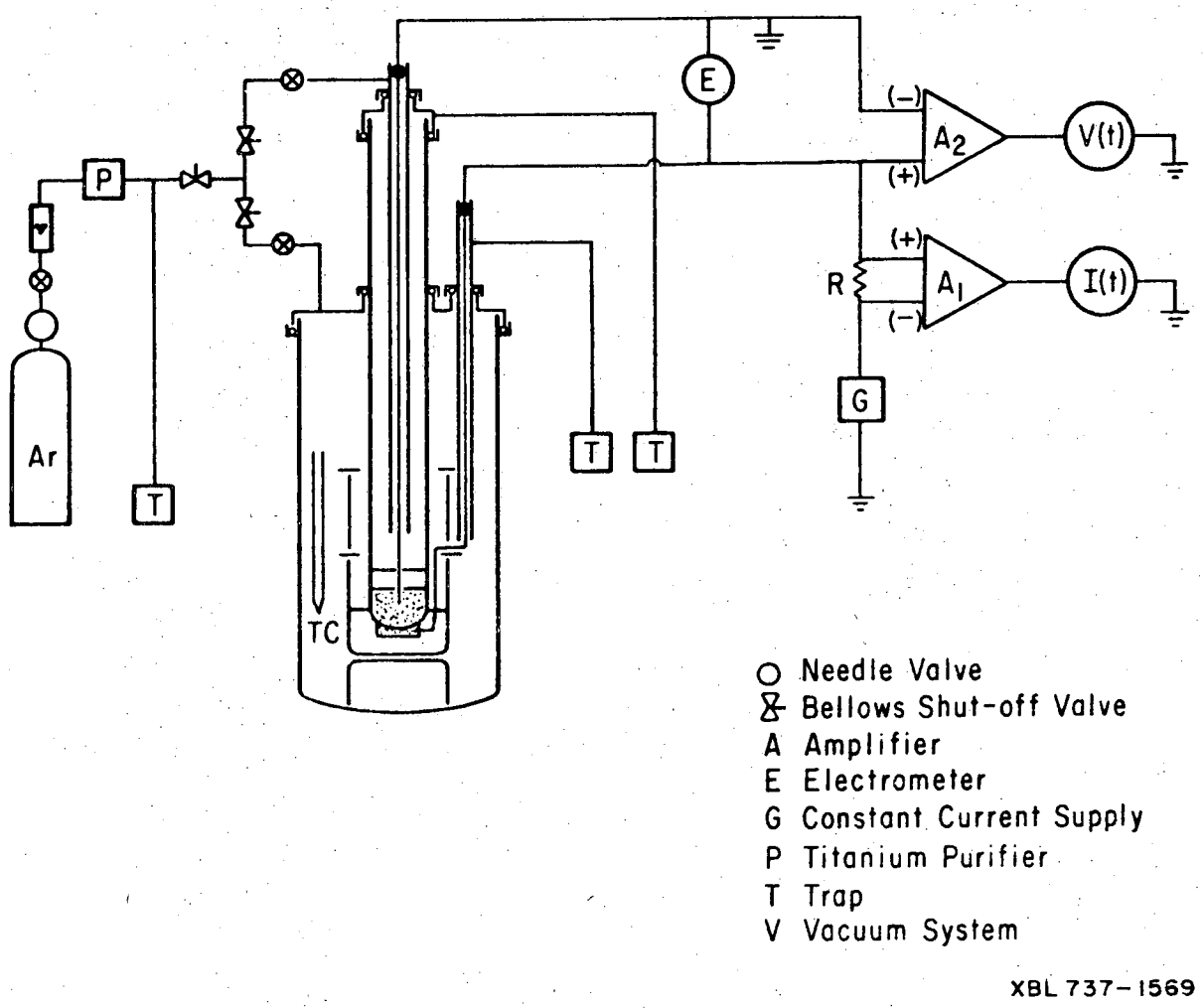
E
(−)
A2
V(t)
(+)
P
(+)
R
A1
I(t)
(−)
G
Ar
T
T
T
TC
○ Needle Valve
⧖ Bellows Shut-off Valve
A Amplifier
E Electrometer
G Constant Current Supply
P Titanium Purifier
T Trap
V Vacuum System
XBL 737-1569

Fig. 2

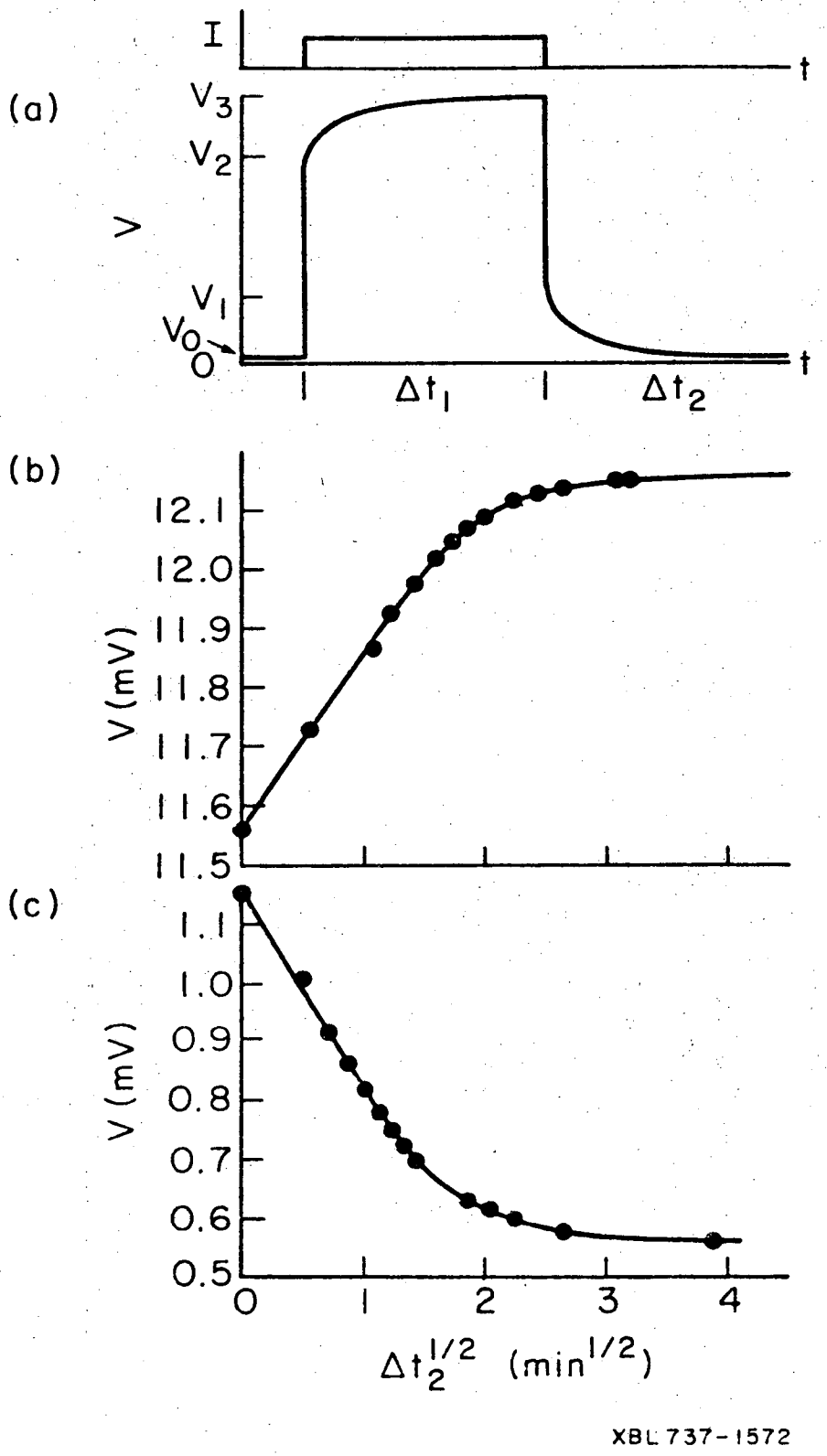
(a)
I
t
V
V_3
V_2
V_1
V_0
0
t
Δt_1
Δt_2
(b)
V (mV)
12.1
12.0
11.9
11.8
11.7
11.6
11.5
(c)
V (mV)
1.1
1.0
0.9
0.8
0.7
0.6
0.5
0
1
2
3
4
$\Delta t_2^{1/2}$ (min$^{1/2}$)
XBL 737-1572

Fig. 3

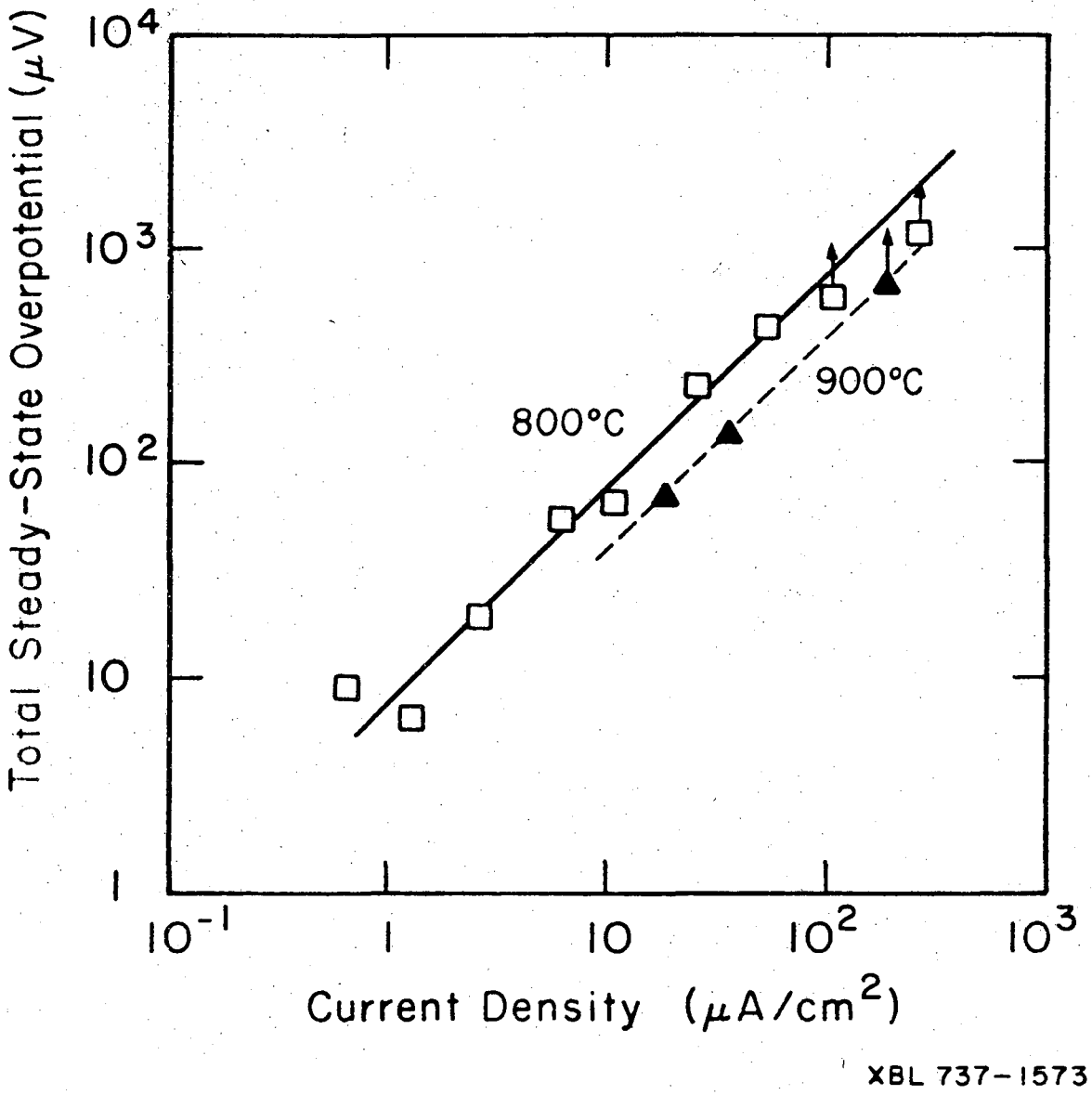
Total Steady-State Overpotential (μV)
10^4
10^3
10^2
10
1
800°C
900°C
10^-1
1
10
10^2
10^3
Current Density (μA/cm^2)
XBL 737-1573

Fig. 4

Mechanism

I. Oxygen solution – diffusion in metal.

II. Oxide nucleation and growth.

III. Oxygen solution – interface diffusion.

IV. $M-MO_n$ – Electrolyte reaction.

V. Anion diffusion in oxide.

VI. Cation diffusion in oxide.

Schematic

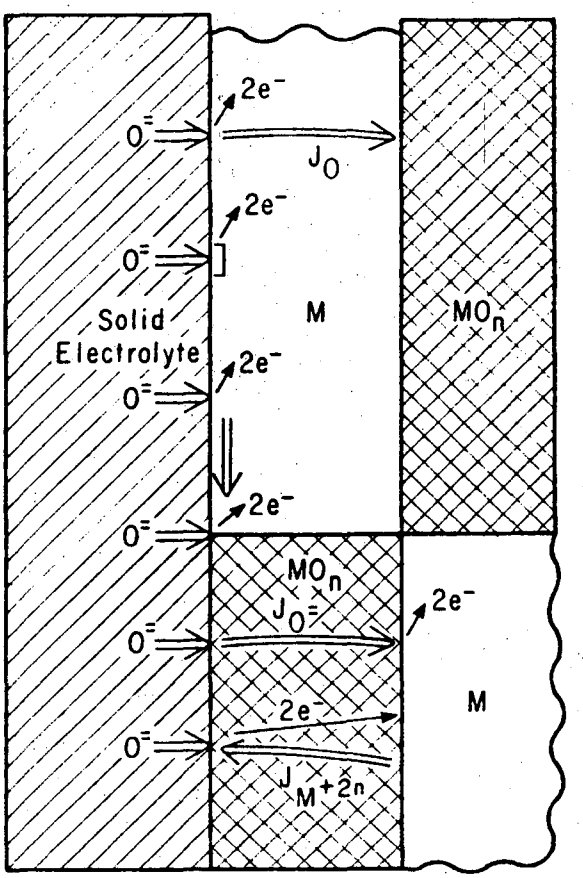

XBL737-1567

Fig. 5

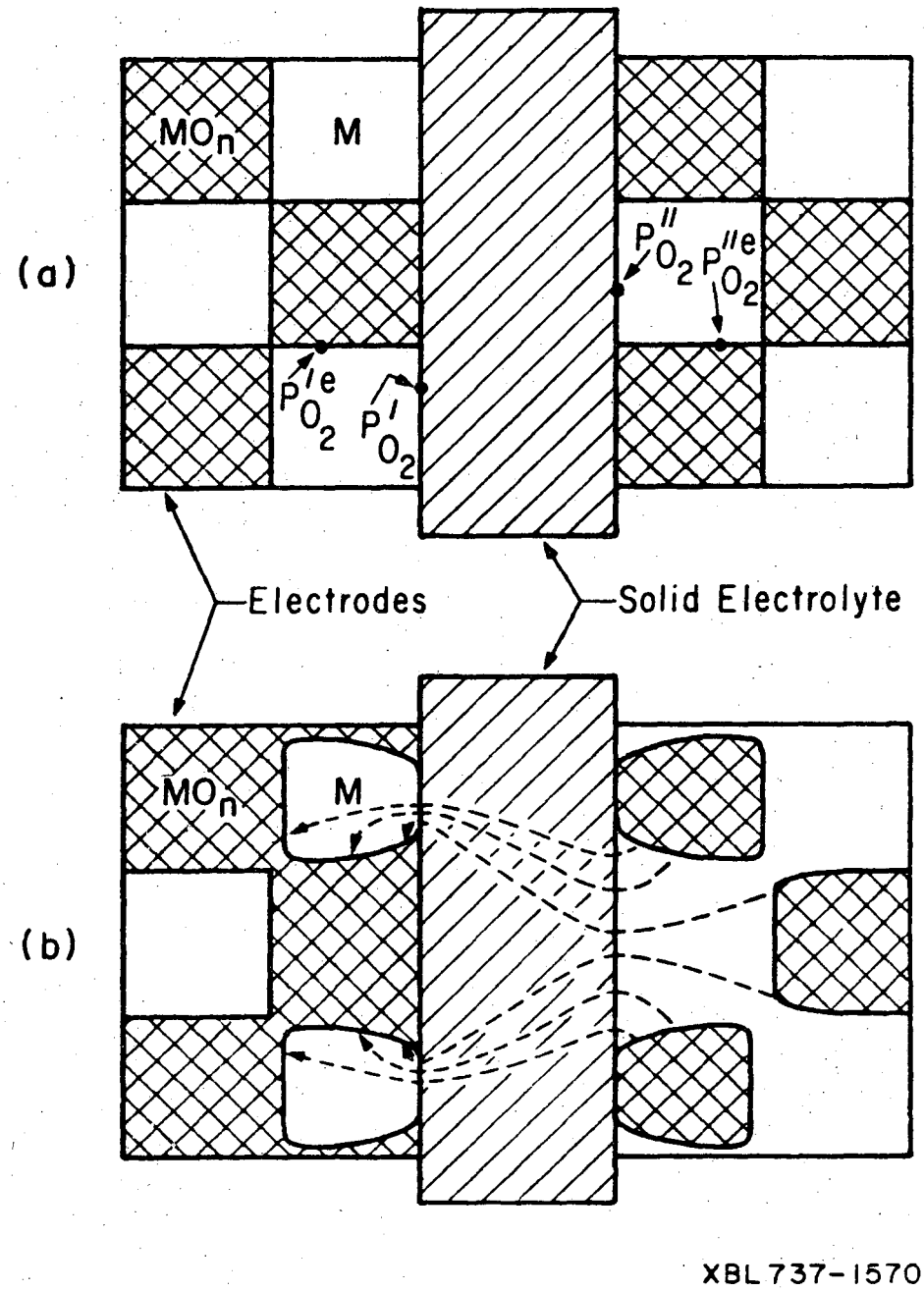

XBL 737-1570

Fig. 6

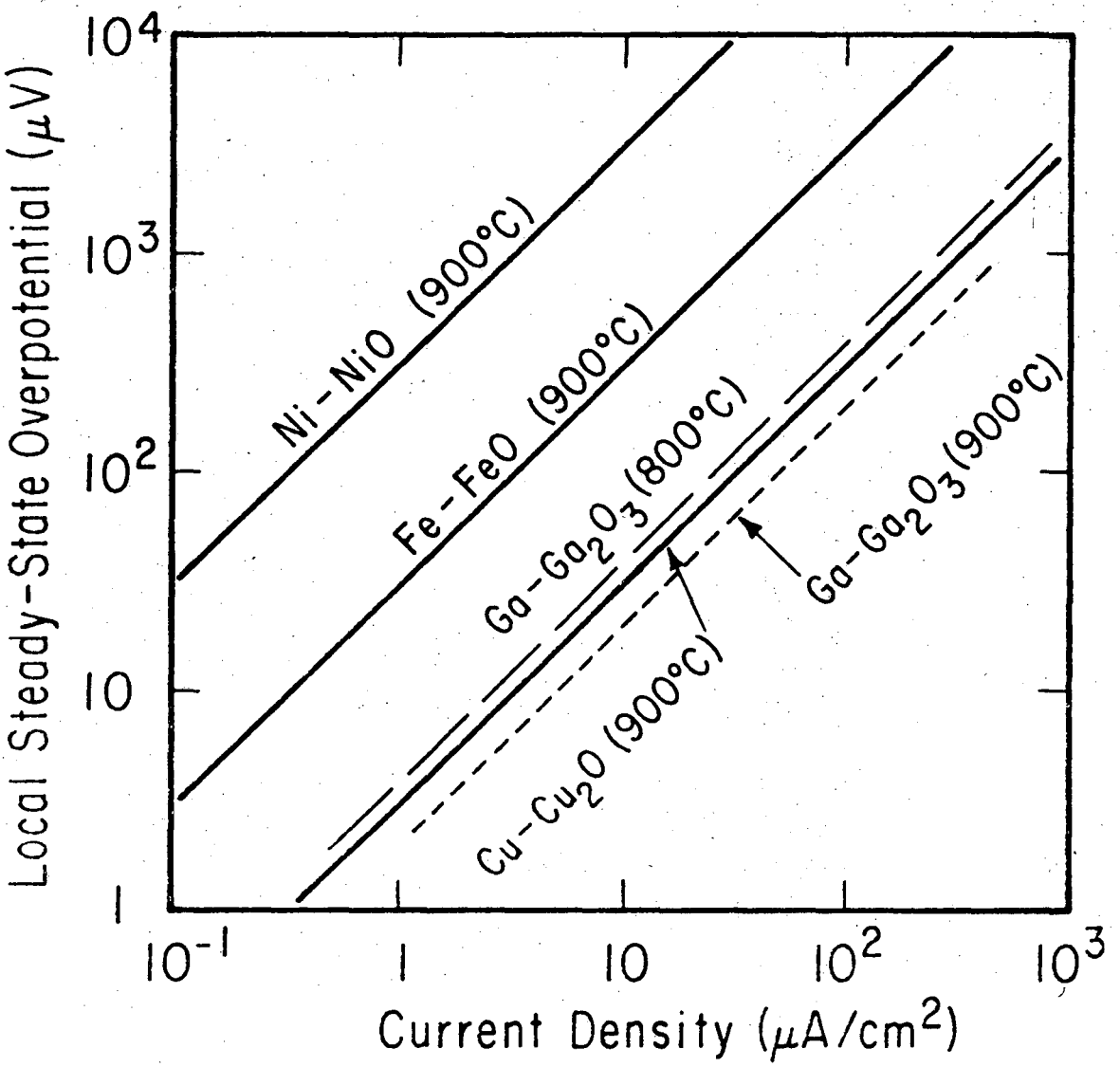

XBL737-1571

Fig. 7

TECHNICAL INFORMATION DIVISION
LAWRENCE BERKELEY LABORATORY
UNIVERSITY OF CALIFORNIA
BERKELEY, CALIFORNIA 94720